On using radial basis functions in a "finite difference mode" with applications to elasticity problems

Article *in* Computational Mechanics · December 2003

DOI: 10.1007/s00466-003-0501-9

CITATIONS
202

READS
547

2 authors, including:

D. A. Shirobokov

20 PUBLICATIONS **298** CITATIONS

SEE PROFILE

Computational Mechanics 33 (2003) 68–79 © Springer-Verlag 2003
DOI 10.1007/s00466-003-0501-9

On using radial basis functions in a "finite difference mode" with applications to elasticity problems

A. I. Tolstykh, D. A. Shirobokov

Abstract A way of using RBF as the basis for PDE's solvers is presented, its essence being constructing approximate formulas for derivatives discretizations based on RBF interpolants with local supports similar to stencils in finite difference methods. Numerical results for different types of elasticity equations showing reasonable accuracy and good *h*-convergence properties of the technique are presented. In particular, examples of RBF solution in the case of non-linear Karman-Fopple equations are considered.

Keywords Radial basis functions, Derivatives discretization, RBF schemes, Solid mechanics equations

1 Introduction

In numerical methods for solid mechanics, the FEM method is universally accepted technique. It allows to exploit unstructured grids thus providing considerable flexibility. However, in the recent years considerable attention was paid to the so called meshless methods which operate with nodes rather than meshes. The motivation came mainly from the following considerations:

- meshless methods do not require grid generation which can be not an easy task in the three dimensional cases;
- meshless methods are more appropriate than FEM or finite difference methods are in the cases of very large mesh deformation and moving discontinuities.

When classifying meshless methods for solving PDEs, at least two approaches can be distinguished:

(i) Methods based on the least squares type of approximations used mainly in the framework of weak formulations, approximated functions and their approximations being distinct at nodes.
(ii) Methods based on the interpolation principle requiring that interpolants are equal to interpolated function at nodes.

Received: 9 December 2002 / Accepted: 11 August 2003
Published online: 20 November 2003

A. I. Tolstykh (✉), D. A. Shirobokov
Computing Center of Russian Academy of Sciences
Vavilova str.,40; Moscow
E-mail: tol@ccas.ru

This work was supported by INTAS, project N1150 and Russian Fund of basic researches, grant 02-01-00436.

To this one can add the so called generalized finite difference method for irregularly spaced nodes [3, 15, 20] which uses multidimensional Taylor expansion series.

There are a lot of methods of type (i) described in the literature (the relevant survey and references can be found, for example, in [4]). As to (ii), it is represented by Radial Basis Functions (RBF) techniques . Considering the latter category, the existence and accuracy of scattered data RBF interpolants are widely discussed. A large body of publications concerning the subject is presented in [13].

The use of RBF for PDEs discretizations offers some nice possibilities. First, some RBF-based discretizations have potential for providing convergence rates dependent on exact solutions smoothness only rather than on degrees of underlying polynomial approximations. In certain cases, they can be exponential.

Second, good RBF performance in three-dimensional cases is theoretically expected.

At present, the most popular lines of attack when constructing RBF-PDE solvers seem to be collocation and boundary elements approaches [7, 8, 12, 31].

In [28, 30] convergence proofs and error estimates of the collocation procedure are presented. A profound impact on the RBF-collocation technique applications is due to papers [12, 14, 21, 27]. In the works, much attention was given to Hardy's multiquadric [11] with varying shape parameters. Dramatic increase of accuracy was found in the case of properly defined shape-parameter distributions.

The main difficulty when using RBF collocation approach is the necessity to invert ill-conditioned matrix arising due to a global RBF support. Several remedies to circumvent the problem were proposed. They are, in particular, domain decomposition approach [27], preconditioning and compactly supported RBF [6, 26, 29].

In [32] the collocation procedure for globally and locally supported RBF were tested against some benchmark problems.

The present papers concerns with another way of using RBF for solving PDEs [24] that is with constructing locally supported operators approximating derivatives in the same manner as in the case of traditional finite difference method.

The essence of the technique is constructing derivatives discretizations based on RBF interpolants for localized sets of nodes which form computational molecules (stencils) similar to those in the case of finite difference approximations. In contrast to the RBF collocations method, governing equations are not satisfied exactly. Instead, they

are approximated at each node with some approximation error. It makes the technique very similar to the finite difference methodology.

The approach seems to possess some merits. They are as follows.

(i) The problem of ill conditioned systems is greatly relaxed due to a limited number of nodes in stencils.
(ii) The technique has the potential for being quite accurate.
(iii) Once RBF coefficients of the derivatives approximation are calculated, the technique can be implemented in a simple manner typical for finite difference schemes.
(iv) The approach offers considerable flexibility by constructing various stencil configurations for different center nodes where derivatives are considered (for example, special configurations near boundaries and singularities).
(v) The resulting RBF schemes can be readily combined with finite differencing schemes in the framework of the domain decomposition strategy.

In [24] approximation orders of the first and second derivatives as functions of distances between nodes for the simplest uniform stencils were investigated. It was found that the functions are, as with finite differences, proportional to some powers of the distances, the powers being increasing with the numbers of nodes in the stencils. It was found also that RBF approximations and high-order compact differencing technique for convection-diffusion equations can go well together in the framework of the domain decomposition approach showing good accuracy when using relatively coarse meshes. As examples, numerical solutions for the 2D Burgers equations in a L-shaped domain were obtained, the RBF and the fifth-order compact difference scheme from [23] being used separately and in concert. In the latter case, the RBF operators served as "interface" discretizations for neighbour subdomains with different meshes.

In the present paper, further results in the area are presented. They concern with applications of the "finite difference mode" of using RBF for solving some elasticity problems, the main emphasis being placed on quantitative estimates of the constructed RBF solvers accuracy.

2
RBF approximations to derivatives and RBF schemes

2.1
RBF approximations to derivatives

Suppose one has a set $X = \{\mathbf{x}_1, \mathbf{x}_2, \ldots, \mathbf{x}_M\} \subset \Omega$ of nodes in a computational domain Ω. Let $X_j = (\mathbf{x}_1^{(j)}, \mathbf{x}_2^{(j)}, \ldots, \mathbf{x}_{N_j}^{(j)})$, $X_j \subset X, \mathbf{x}_j \in X_j$ be a "cloud" of nodes surrounding each node $\mathbf{x_j}$. The node will be referred to as a center of the cloud. Following finite difference terminology, we shall however use the notion "stencil" instead of cloud.

Suppose further that $u(\mathbf{x}), \mathbf{x} \in \Omega$ is a sufficiently smooth function. Denoting $u(\mathbf{x_i}) = u_i$, let us introduce "internal" numbering for a subset X_j: if $\mathbf{x}_i = \mathbf{x}_k^{(j)}$ then $u_i = u_k^{(j)}$ where k is some number from $(1, 2, \ldots, N_j)$.

We construct for each X_j an interpolant

$$s^{(j)}(\mathbf{x}) = \sum_{k=1}^{N_j} c_k^{(j)} \phi(||\mathbf{x} - \mathbf{x}_k^{(j)}||) + \mathrm{d}, \quad \mathrm{d} = \mathrm{const},$$
$$c_k^{(j)} = \sum_{i=1}^{N_j} b_{ki}^{(j)} u_i^{(j)} \tag{1}$$

where $b_{ki}^{(j)}$ are the entries of the matrix which is inverse of the coefficients matrix $A^{(j)}$ arising from the interpolation conditions $s^{(j)}(\mathbf{x}_k^{(j)}) = u_k^{(j)}, k = 1, 2, \ldots, N_j$ and the additional condition $\sum_{i=k}^{N_j} c_k^{(j)} = 0$ needed if $\mathrm{d} \neq 0$.

For any linear operator D we construct the approximate formula $[Du]_j \approx \sum_{k=1}^{N_j} c_k^{(j)} [D\phi(||\mathbf{x} - \mathbf{x}_k^{(j)}||)]_j$ where the notation $[Du]_j = Du|_{\mathbf{x}=\mathbf{x_j}}$ is used. Substituting the expression for $c_k^{(j)}$, one may write finally

$$[Du]_j \approx \sum_{i=1}^{N_j} (c_D)_i^{(j)} u_i^{(j)}$$
$$(c_D)_i^{(j)} = \sum_{k=1}^{N_j} b_{ki}^{(j)} [D\phi(||\mathbf{x} - \mathbf{x}_k^{(j)}||)]_j, \quad j = 1, 2, \ldots, M \tag{2}$$

The coefficients $(c_D)_i^{(j)}$ depend only on D and the coordinates of the nodes belonging to the j-th stencil. They do not vary during the solution processes (if nodes are not moving) and can be calculated during preprocessing.

In the following, we shall suppose that D is an operator of derivatives in respect to Cartesian coordinates. Then (2) may be viewed as usual numerical differentiation formulas written for stencils X_j. Using such formulas for discretizations of PDE's when each internal node considered as a center leads to algebraic systems with sparse matrices typical for a conventional finite difference method. It is worth noting that it is possible to use "oriented" stencils for skew-symmetric operators thus introducing an upwinding.

We shall be interested further in the actual accuracy of (2) in the cases when D is the operator of first or second partial derivatives and N_j are reasonably small numbers. There are some estimates of the h-convergence in the case of cardinal interpolation [16] when nodes $\mathbf{x}_j$ are generated by the Cartesian grid with $N_j = \infty$. A natural but not general way to estimate the approximation errors for relatively small N_j is their direct calculations for certain classes of functions. Of course, it gives only some impression concerning the RBF performance in a finite difference mode. The results of the calculations for Hardy multiquadrics (MQ)

$$\phi(r) = (r^2 + C)^{1/2} \ , \tag{3}$$

with $\mathrm{d} \neq 0$ are presented in [24]. Figure 1 shows L_2 - norms of errors in the case of first and second derivatives of $u(x) = \exp(2(x + y))$ when using the stencils indicated herein.

It can be seen from Fig. 1 that the norms can be well presented by the power laws h^p where h is the distance between nodes while $p = 2, 4, 6$ for stencils 1, 2, 3. For a fixed $h = h_*$, enlarging stencils increases the accuracy of the derivatives discretization. However, one should not expect that this will continue when the number of nodes

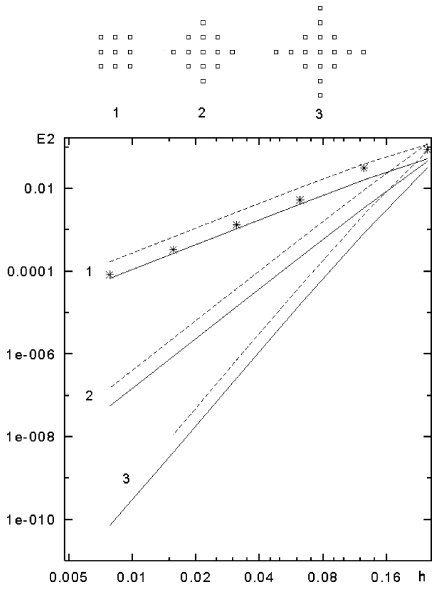

Fig. 1. Mean-root-square errors vs. mesh size and the corresponding RBF stencils. Solid and dashed lines correspond to first and second derivatives

$N_j = K$ in the stencils increases without bound. When $K \to \infty$, the accuracy of the interpolation which provides differencing formulas is expected to tend to that of the cardinal interpolation [5] for $h = h_*$.

In the figure, the result obtained with the second-order-accurate centered finite difference formula for the first derivative are also shown. They are close to those for the stencil 1.

We consider here more general formulas of the Hermitian type. Suppose that values $f_i = f(\mathbf{x}_i^{(j)})$ are specified at some nodes of the jth stencil $\mathbf{x}_1^{(j)}, \mathbf{x}_2^{(j)}, \ldots, \mathbf{x}_p^{(j)}$ while functionals $Lf|_{\mathbf{x}=\mathbf{x}_k^{(j)}}$ are given at $\bar{\mathbf{x}}_1^{(j)}, \bar{\mathbf{x}}_2^{(j)}, \ldots, \bar{\mathbf{x}}_q^{(j)}$ where L is a linear operator. It is assumed that $\mathbf{x}_i^{(j)}$ and $\bar{\mathbf{x}}_k^{(j)}$ are possibly coincide for certain i and k.

We construct the interpolant

$$s^{(j)}(\mathbf{x}) = \sum_{k=1}^{p} a_k \phi(||\mathbf{x} - \mathbf{x}_k^{(j)}||) + \sum_{k=1}^{q} b_k L\phi(||\mathbf{x} - \bar{\mathbf{x}}_k^{(j)}||),$$
$$p, q < N_j \ ,$$

where L acts on ϕ as a function of $\mathbf{x}$. Requiring that

$$s^{(j)}(\mathbf{x}_k^{(j)}) = f(\mathbf{x}_k^{(j)}),$$
$$Ls^{(j)}|_{\mathbf{x}=\bar{\mathbf{x}}_k^{(j)}} = Lf|_{\mathbf{x}=\bar{\mathbf{x}}_k^{(j)}} = Lf_k$$

one obtains the following linear system

$$\begin{pmatrix} \phi_{11} \ldots \phi_{1p} & L\phi_{11} \ldots L\phi_{1q} \\ \vdots & \vdots \\ \phi_{p1} \ldots \phi_{pp} & L\phi_{p1} \ldots L\phi_{pq} \\ L\phi_{11} \ldots L\phi_{1p} & L^2\phi_{11} \ldots L^2\phi_{1q} \\ \vdots & \vdots \\ L\phi_{q1} \ldots L\phi_{qp} & L^2\phi_{q1} \ldots L^2\phi_{qq} \end{pmatrix} \begin{pmatrix} a_1 \\ \vdots \\ a_p \\ b_1 \\ \vdots \\ b_q \end{pmatrix} = \begin{pmatrix} f_1 \\ \vdots \\ f_p \\ Lf_1 \\ \vdots \\ Lf_q \end{pmatrix} \quad (4)$$

$$\phi_{ij} = \phi(||\mathbf{x}_i - \mathbf{x}_j||), L\phi_{ij} = L\phi(||\mathbf{x} - \mathbf{x}_j||)|_{\mathbf{x}=\mathbf{x}_i},$$
$$L^2\phi_{ij} = L^2\phi(||\mathbf{x} - \mathbf{x}_j||)|_{\mathbf{x}=\mathbf{x}_i} \ .$$

Assuming that matrix (4) does not degenerate (this is the case for certain types of ϕ), one can solve the system for coefficients a_k, b_k. In particular, the system is solvable for (3).

Supposing that D_α is the operator of α-th derivatives at a node $\mathbf{x}_j$ and applying it to $s^{(j)}(\mathbf{x})$, one obtains the following generalization of (2):

$$D_\alpha f \approx \sum_{k=1}^{p} C_k^{(\alpha)} f_k + \sum_{k=1}^{q} B_k^{(\alpha)} Lf_k \ , \quad (5)$$

where the coefficients $C_k^{(\alpha)}$ and $B_k^{(\alpha)}$ depend on the coordinates of the nodes forming j-th stencil.

Particular forms of Eq. (2) can be used for approximations to derivatives in governing equations. For example, a discrete forms of the first and second order derivatives of a function for j-th node with a stencil S_j read

$$\left(\frac{\partial u}{\partial x}\right)_j \approx \sum_{i \in I(S_j)} c_{xi}^{(j)} u_i^{(j)}, \quad \left(\frac{\partial^2 u}{\partial x^2}\right)_j \approx \sum_{i \in I(S_j)} c_{xxi}^{(j)} u_i^{(j)} \ ,$$

where $I(S_j)$ is the index set corresponding to S_j while $c_{xi}^{(j)}$ and $c_{xxi}^{(j)}$ are the RBF x-derivatives coefficients for jth stencil. Similar formulas can be constructed for higher derivatives. However, they can be also approximated by successive applications of RBF operators for lower order derivatives. For example, $\partial^4 u/\partial x^4$ can be discretized in the form

$$\left(\frac{\partial^4 u}{\partial x^4}\right)_j \approx \sum_{i \in I(S_j)} c_{xxi}^{(j)} \sum_{k \in I(S_i)} c_{xxk}^{(i)} u_k^{(i)}$$

where S_i is a stencil for i-th node of S_j.

One may also need derivatives discretizations near boundary nodes with the Neumann-type boundary conditions. A particular form of Eq. (5) can be written in this case as

$$D_\alpha u_j \approx \sum_{i \in I(S_j^*)} C_i^{(\alpha)(j)} u_i^{(j)} + \sum_{i \in I(S_j^* \cap \Gamma)} B_i^{(\alpha)(j)} (\partial u/\partial n)_i^{(j)}$$

where Γ is a boundary and $(\partial u/\partial n)_i^{(j)}$ is the normal to Γ derivative.

When introducing the above formulas, it is supposed that u_i is a restriction of a sufficiently smooth function $u(x)$. In the case of singular points, it is possible to modify the interpolant $s(x)$ in Eq. (1) for stencil near singularities.

2.2 RBF schemes

Discretization at each node of a given PDE can be proceeded in a standard finite difference manner by changing derivatives by their approximations. Assembling then the resulting algebraic equations and using boundary conditions (which if needed, can be discretized as well), one obtains a global system for unknown nodal variables.

In the linear case, its matrix is a sparse one and the system can be solved using direct or iterative methods. In

the numerical experiments described below the direct nested dissection method [9] was used. It should be noted that condition numbers for "global" systems were found to be quite acceptable. However, though the present technique suggests $N_j << N$, ill-conditioning of system like (4) can not be ruled out if N_j is too large or distances between nodes are too small. In the calculations, the situation has been encountered only in the h-convergence studies when very small values of h, the characteristic distances between nodes, were used. In those cases, quadro precision arithmetic was exploited. The preconditioning ideas of [2] seems to be quite attractive to deal with such cases.

Summing up, to solve a PDE using the present RBF approach, one should:

(i) Specify a nodes distribution in the considered computational domain;
(ii) For each node x_j considered as a center, specify a stencil with N_j nodes surrounding x_j;
(iii) For each stencil, obtain "differencing" coefficients (for example $(c_D)_i^{(j)}$ in (2)) by solving linear systems;
(iv) Substitute the approximations to derivatives at each node in the PDE and form the resulting "global" system by assembling together the nodal approximations;
(v) Solve the global system.

It should be noted that steps (i)–(iii) can be viewed as a preprocessing procedure once nodes distributions and stencils are not supposed to be changed during calculations. In nonlinear cases, only steps (iv) and (v) have to be included in iterations.

As in the case of finite difference schemes, it can be easily shown that the method written in the form

$$L_h u_h = f_h$$

where $L_h : U_h \to F_h, u_h \in U_h, f_h \in F_h$ and f_h are an operator of a RBF scheme and U_h, F_h are spaces of unknown and given nodal functions respectively, provides convergence of an order k,that is

$$||[u]_h - u_h||_{U_h} < Ch^k$$

for fixed stencils if the following holds:

(i) $||L_h[u]_h - f_h||_{F_h} < C_1 h^k$
(ii) $||u_h - v_h||_{U_h} < C_2 ||\delta_h||_{F_h}$

In the above inequalities expressing approximation and stability properties, $[\cdot]_h : U \to U_h$ is a projection operator, U is a space to which belongs the exact solution u, v_h satisfies $L_h v_h = f_h + \delta_h$ and constants C, C_1, C_2 are independent of h.

Unfortunately, it is difficult to prove both (i) and (ii) in a general case of arbitrary spaced nodes and arbitrary stencils. However, the potential for satisfying (i) and (ii) was discussed in [24] where it was shown that the RBF approximation to the Laplace operator using stencil 1 from Fig. 1 is a negative definite one (the Hilbert space of double-periodic nodal functions with the inner product $(u, v) = h^2 \sum_{i,j} u_{ij} v_{ij}$ where u_{ij} and v_{ij} are defined at grid points $x_i = ih, y_j = jh$ of the Cartesian grid was assumed). As a result, in that case (as well as in the cases of other stencils shown in Fig. 1), very fast convergence was observed when using the simplest iterative procedure for inverting the corresponding L_h operators.

In the calculations described below, h-convergence was always seen at least for the considered ranges of h and all considered stencils.

Though general RBF methodology is really meshless one and a random nodes distribution can be used, the most accurate numerical solutions can be expected only if a "proper" distribution is specified depending on the problem to be solved. Moreover, the strategy of choosing stencils in the present approach, as in finite difference methods, plays an important role.

Since the presented below calculations are aimed mainly at comparisons with other methods, either triangulated or Cartesian meshes were served as nodes distributions. As to step (ii), different strategies were used when specifying stencils.

In the following, the MQ radial basis functions will be considered only. We set $C = 1$ in (3) when carrying out the majority of the descried below calculations since we are not aware of the existence of a theory giving an optimal choice of C. Of course, judging from the results presented in [12, 14] the solutions accuracy is expected to be poorer than that for a more successful choice of C.

3
Testing calculations for linear problems

To investigate performances of schemes based on RBF discretizations of derivatives, the technique was applied to the following typical testing problems described by different types of equations:

(i) The Dirichlet's problem for the Poisson equations which is relevant, in particular, to bars torsion calculations. In the context of RBF, the collocation method is commonly used to solve the problem.
(ii) A boundary-value problem for the biharmonic equation describing the Kirchgoff plates bending.
(iii) Elasto-static problems described by the plane stresses formulation.

As RBF nodes, those of meshes usually adopted for FD and FEM calculations were used thus facilitating comparisons of solutions on equal terms.

Several strategies of constructing stencils were considered. In cases (i) and (ii), the consideration was restricted to two types of supports for each center nodes with 7 and 19 neighbour points supplied by triangulated meshes. They are expected to provide 2nd- and 4th- order h-convergence respectively. Of course, a rich variety of other stencils can be used when solving the problems. In case (iii), the strategy was to select nodes falling into prescribed geometrical forms (squares, ellipses etc.).

The FEM solutions used for comparison were either extracted from the relevant literature or calculated in the framework of the present investigation. In the latter case, the simplest triangular elements with the weak formulation as described in [17] were used to solve the Poisson equations, the biharmonic operator being considered as the product of two Laplace operators. The

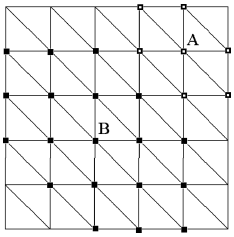

Fig. 2. A triangulated mesh in a square domain. The "simple" stencil for the node A and the "enlarged" stencil for the node B are shown by white and black markers respectively

solutions do not characterize the performance of sophisticated FEM versions and served only as reference ones.

3.1
Dirichlet problem for Poisson equations

We consider first the RBF solutions of the Poisson equation

$$\triangle u = f(x,y) = -2\pi^2 \sin \pi x \sin \pi y$$

in the square $\Omega = \{0 < x < 1,\ \ 0 < y < 1\}$ assuming zero boundary conditions. The exact solution is $u = \sin \pi x \sin \pi y$.

The coordinates of the nodes were taken as $(hi, hj),\ 0 \le i \le l,\ \ 0 \le j \le l$ where l is an integer and $h = 1/l$ is the size of the triangulated mesh (Fig. 2). Two types of stencils were used to estimate possible performance of the technique, namely, "simple" and "enlarged" ones.

The first stencil with node A as a center (Fig. 2) includes the node and its nearest neighbors. The second one (node B is a center, Fig. 2) contains the nodes of the first stencils and additionally those nodes which are connected with them by triangle's sides. In this way, seven and nineteen nodes respectively form the stencils away from boundaries. Near the boundaries, the enlarged stencils contain smaller numbers of nodes.

Let $u_j,\ j = 1, \ldots, (l+1)^2$ be a function defined at the nodes in the computational domain. Then the RBF approximation to the governing equation at a j-th internal node looks as

$$\sum_{i \in I(S_j)} (c_{xxi}^{(j)} + c_{yyi}^{(j)}) u_i = f(x_j, y_j)$$

where the summation is performed over the set S_j of nodes belonging to the stencil with the center in the jth node while $c_{xxi}^{(j)}$ and $c_{yyi}^{(j)}$ $(i \in I(S_j))$ are the coefficients of the second derivatives approximation corresponding to the x and y coordinates respectively. Adding the boundary conditions $u_j = 0$, $\mathbf{x_j} \in \partial\Omega$, one obtains a linear system with a sparse matrix.

Figure 3 shows L_2 norms of the solutions errors for the "simple"(RBF-1) and "enlarged"(RBF-2) stencils as functions of the mesh size. For comparison, the results for the FEM method from [17] with linear elements as well as the fourth-order finite-difference scheme based on compact differencing are also presented in the Figure.

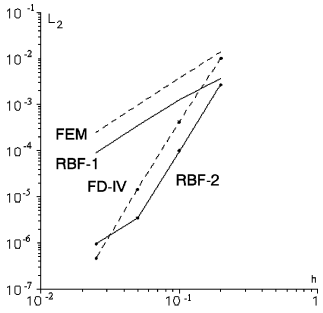

Fig. 3. Mean-root-square errors vs. mesh size for the Dirichlet problem. RBF-1 and RBF-2 curves correspond to "simple" and "enlarged" stencils respectively. FEM curve corresponds to linear triangular elements for the Poisson equations solved successively. FD-IV curve corresponds to the fourth-order compact difference schemes

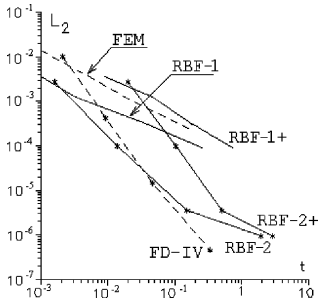

Fig. 4. Mean-root-square errors vs. CPU time measured in reference units for the Dirichlet problem in the square domain. RBF-1 (RBF-1+) and RBF-2 (RBF-2+) curves correspond "simple" and "enlarged" stencils with excluding (including) computational expenses needed to calculate RBF coefficients

As can be seen, RBF-1 and RBF-2 discretizations show second- and fourth-order convergence respectively, the latter being slightly more accurate than finite difference one. Some decrease of accuracy of the RBF-2 solution seen in the finest mesh region is perhaps due to the deterioration of the condition number of the linear systems defining the RBF operator.

In Fig. 4, L_2 norms of the solutions errors are presented as functions of CPU time needed to solve the problem. The estimates for the RBF computational time were obtained with including and excluding the time needed to calculate the RBF coefficients in the framework of the preprocessing procedure. The latter type of estimates makes sense since they are applicable, for example, to non-linear problems requiring iterations. In that case, one can use for many times RBF coefficients preliminary calculated and stored.

For comparison purposes, the results for the fourth-order compact difference scheme and the above mentioned FEM version are also shown in Fig. 4. It should be noted that, as can be readily shown, the linear systems for the present FEM and uniform meshes are identical to those for five-point finite-difference method.

As evident from the Figure, using the RBF with the seven nodes "simple" stencil require slightly more time

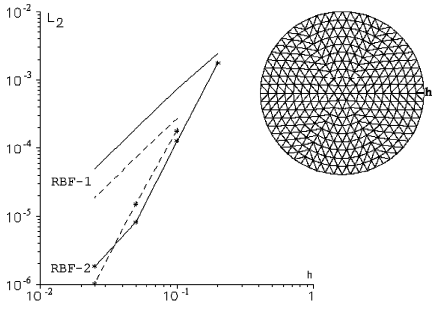

Fig. 5. Mean-root-square errors vs. mesh size for the Dirichlet problem in the unit circle (solid lines) and circle with a hole (dashed lines). RBF-1 and RBF-2 labels are defined in Fig. 3

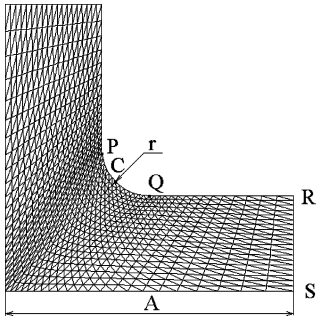

Fig. 6. L-shaped domain with rounded incoming corner

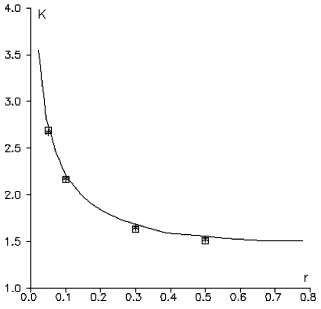

Fig. 7. The stress concentration parameter K vs. radius of the rounding

than the present FEM if the RBF coefficients should be calculated for each node. On the contrary, it is advantageous if the coefficients are supposed to be known. The same conclusion can be drawn if they are calculated in a parallel manner using parallel machines. It can be seen also that the RBF efficiency considerably increases in the present case when using the "enlarged" stencil.

Comparisons with exact solutions (that is, L_2 numerical solution errors) for domains with circular boundaries are presented in Fig. 5. An example of triangulated meshes used in the calculations is shown in Fig. 5, the mesh size h being assumed to be the distance between co-centered circles. Two cases are considered. The first one corresponds to the Dirichlet problem for the circle $0 < r < 1$ and the right-hand side $f = 5r \sin 2\phi$ where (r, ϕ) are the polar coordinates, the exact solution being $u = (r^3 - r^2) \sin 2\phi$. In the second case, the domain looks as the unit circle with the hole $1/2 < r < 1$. The exact solution for the considered $f = (5r - 3/(2r)) \sin 2\phi$ is $u = r(r^2 - 3r/2 + 1/2) \sin 2\phi$.

As Fig. 5 suggests, both RBF-1 and RBF-2 curves can preserve the second- and fourth-order of their h-convergence respectively in the cases of more complicated geometries.

3.2
Torsion of prismatic bars

According to the elasticity theory, solutions of the bar torsion problem can be obtained by solving the Dirichlet problem for the Poisson equation

$$\triangle\phi = -2, \quad \mathbf{x} \in \Omega, \quad \phi|_{\partial\Omega} = \mathbf{0}$$

where Ω is a bar cross-section domain. The corresponding stress components can then be expressed in terms of x- and y-derivatives of ϕ. In the case of cross-sections which boundaries contain "incoming" angles with rounded vertices, it is of interest to predict accurately stress concentrations near rounded corners where high gradients are possible (it has been known that stresses become singular when the corresponding curvature radii tend to zero).

We consider the geometry of a bar cross-section shown in Fig. 6 which was investigated in [25] using very accurate semi-analytic method. The cross section is characterized by the radius r of the rounded corner and the "shelf" length A, the shelf thickness being assumed to be unity. The asymptotics in the case $r \to 0$ was investigated in [17, 25]. To describe properly stresses near point C for small r, high-accuracy methods are needed.

The RBF calculations were carried out using triangulated meshes (one of them is shown in Fig. 6). The meshes are defined by numbers M and N of nodes uniformly distributed along the boundary PQ and the boundary RS respectively. Thus the condensing of nodes near C can be achieved by increasing M. The mesh shown in Fig. 6 is defined by $M = 11$, $N = 20$.

To compare the solution $K = \text{grad}\phi$ gradient in C with the results of [25], the ϕ derivatives were approximated using the third-order four-points formula. The calculations carried out for three meshes $M = 11$, $N = 20$, $M = 21$, $N = 40$ and $M = 41$, $N = 80$ showed that the difference between the results corresponding to the second and the third meshes can be estimated as 0.2%.

Figure 7 displays the K values obtained for $A = 3$ and $r = 0.5, 0.3, 0.1, 0.05$ using the "simple" stencil defined on the coarsest mesh (markers as squares) and finest mesh (markers as stars), the difference between the values being about 1.2% (an exception is the case $r = 0.05$).

The curve depicted in Fig. 7 corresponds to the "almost exact" solution [25] for $A = \infty$. Since the influence of A is quite insignificant in the domain $A > 3$ (the results for $A = 3$ and $A = 4$ differs by 0.2%), the agreement is rather good.

Another comparison with the solution from [25] are shown in Fig. 8. In the Figure, the ratio K/A for the fixed value $r/A = 0.1$ is presented as a function of $1/A$. Again that the present results (markers) agree closely with those from [25] (solid line).

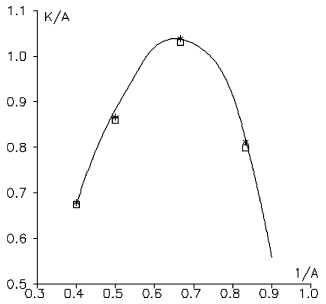

Fig. 8. The parameter K/A vs. $1/A$. The solid line and markers correspond to results from [25] and the present results

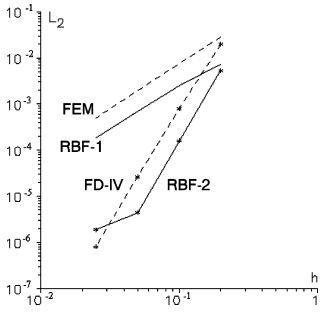

Fig. 9. Mean-root-square errors vs. mesh size for the biharmonic equation in a square domain. FEM, RBF-1, RBF-2 and FD-IV labels are defined in Fig. 3

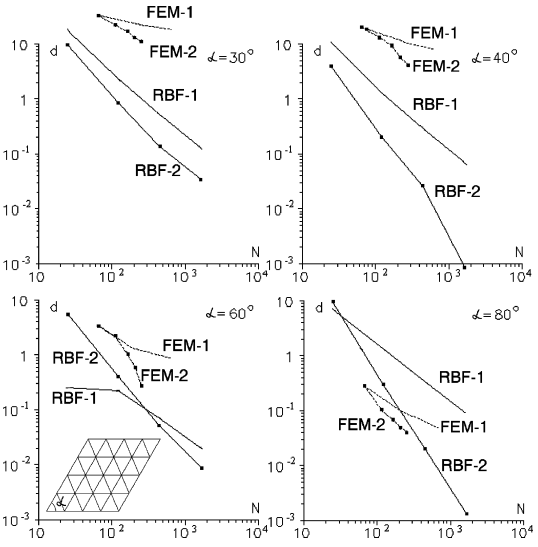

Fig. 10. Relative center displacement error for rhombic plate vs. number of nodes. RBF-1 and RBF-2 labels are defined in Fig. 3. FEM-1 and FEM-2 curves correspond to degrees of freedom element [1] with uniform and condensed near singularities mesh points respectively

3.3
Application to plates

We consider below two cases of the Kirchgoff plates for which exact solutions are available. Their bending is described by the biharmonic equation. In the particular case of simply supported edges, a solution procedure can be reduced to successive solutions of two Poisson equations.

Consider the solution of the biharmonic equation in the domain $0 < x < 1,\ \ 0 < y < 1$ assuming its right hand side to be $4\pi^4 \sin \pi x \sin \pi y$ (which is proportional to a plate loading). Assuming also the boundary conditions $u|_\Gamma = \partial^2 u/\partial n^2|_\Gamma = 0$ where Γ is the domain boundary, the exact solution is $u = \sin \pi x \sin \pi y$. The case corresponds to simply supported edges.

Figure 9 presents the mean square root of the numerical solution errors as functions of the triangulated mesh size for the "simple" RBF-1 and "enlarged" RBF-2 stencils. The results obtained with the FEM method from [17] and with the fourth-order compact differencing technique are also presented in the Figure. It can be seen that, as for the Dirichlet's problem for the Poisson equation, the "simple" and "enlarged" stencils show the second- and the fourth-order mesh-convergence. Moreover, the present RBF technique turns out to be more accurate than FEM even if the "simple" stencil is used.

As the next testing example, we consider bending of a simply supported rhombic plate subject to an uniform load. In this case, there is a singularity of the exact solution which has an adverse effect on accuracy of a numerical method due to decreasing its smoothness with decreasing the angle $\alpha, \alpha < \pi/2$ of the rhomb. The problem is investigated in [1] in the context of several finite element methods performances using the variational approach rather than the biharmonic equation.

Figure 10 displays the relative center displacement errors (on a percentage basis) vs. the number of nodes in the computational domain. The exact solution considered as a reference one was obtained using the technique described in [19]. The RBF results were obtained for four values of the angle α. They are compared with the FEM results from [1].

It should be noted that, instead of the successive inversions of the two discretized Laplace operators, one can use RBF discretizations of the fourth-order derivatives appearing in the biharmonic equations. In the case of the considered rhombic plates, it gives exactly the results presented in Fig. 10.

3.4
Cantilever beam and infinite plate with a hole

Consider now the application of the described approach to 2D elasto-statics problems, namely a cantilever beam and an infinite plate with a hole, which are popular when verifying meshless methods (see for example [4], [32]). The governing equations this time are

$$\frac{\partial \sigma_{xx}}{\partial x} + \frac{\partial \sigma_{xy}}{\partial y} = 0, \quad \frac{\partial \sigma_{xy}}{\partial x} + \frac{\partial \sigma_{yy}}{\partial y} = 0$$

where, assuming plane-stress case

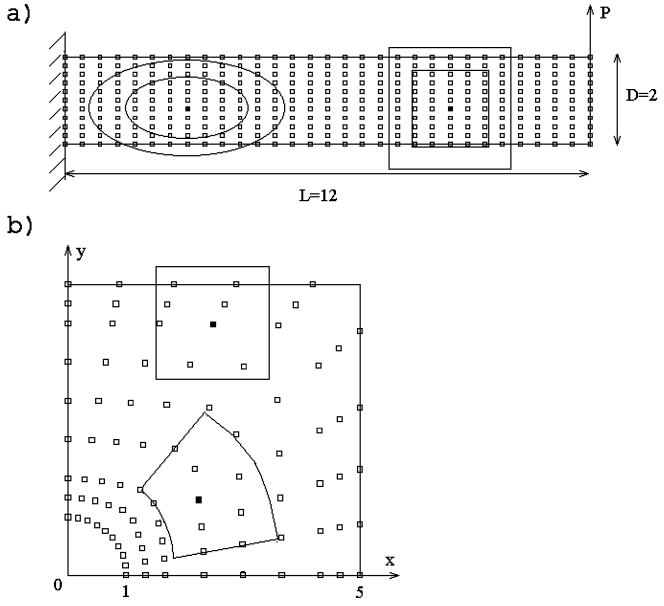

Fig. 11. Computational domains and RBF supports for elastostatic problems **a** cantilever beam, **b** plate with a hole

$$\sigma_{xx} = \frac{E}{1-v^2}\left(\frac{\partial u}{\partial x} + v\frac{\partial v}{\partial y}\right), \quad \sigma_{xy} = \frac{E}{2(1+v)}\left(\frac{\partial u}{\partial y} + \frac{\partial v}{\partial x}\right),$$
$$\sigma_{yy} = \frac{E}{1-v^2}\left(\frac{\partial v}{\partial y} + v\frac{\partial u}{\partial x}\right)$$

and u, v are displacements in the x- and y-directions and E is the elastic modulus, v is the Poisson's ratio. In both cases (beam and plate) we set $E = 1000$, $v = 0.3$ as in [32]. As boundary conditions, the displacements defined by the exact solutions were used. The exact solution for the cantilever beam problem can be found in [22]. It reads

$$u = -\frac{P}{6EI}(y - D/2)\left[(6L - 3x)x + (2+v)(y^2 - Dy)\right]$$

$$v = \frac{P}{6EI}\left[3v(y - D/2)^2(L - x) + (4 + 5v)D^2x/4 + (3L - x)x^2\right]$$

where I is the moment of inertia and the force P is indicated in Fig. 11a.

They were approximated at nodal points which were distributed in the same manner as those in the above cited publications. Though an optimal choice of stencils is beyond the scope of the present paper, different strategies of their forming were tried. One of them was as follows. For each center $\mathbf{x}_j$, the stencil was defined as a set of nodes which fall on a domain $S_j : \mathbf{x}_j \in S_j$ with a prescribed shape of its boundary and a prescribed characteristic length R (the latter was, for example, the edge of a square etc.) or a characteristic area.

In the cantilever beam case, grid points of regular $M \times N$ meshes were used as nodes. The beam length and width are $L = 12$ and $D = 2$ respectively. The geometry of the computational domain, the nodes spacing and examples of supports (ellipses and squares) are shown in Fig. 11a.

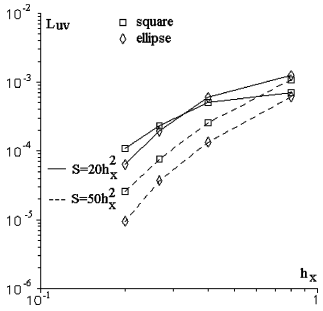

Fig. 12. The cantilever beam problem: relative errors of displacements vs. mesh size h_x for two supports shown in Fig. 11 and their areas S of supports

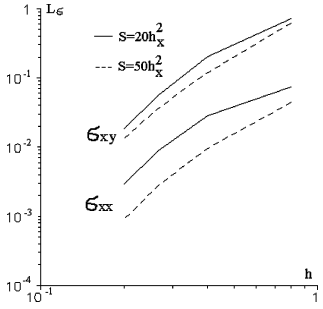

Fig. 13. The cantilever beam problem: relative errors of stresses vs. mesh size h_x for two areas of ellipsis

Figure 12 presents L_{uv} solution errors as functions of the mesh size h_x in the x-direction for stencils which nodes fall on squares and ellipses with the axis length ratio 2 : 1, the area of the supports being $20h_x^2$ and $50h_x^2$. The L_{uv} errors are defined as

$$L_{uv} = \left(\frac{\sum_i (u_i - u_{ei})^2 + (v_i - v_{ei})^2}{\sum_i u_{ei}^2 + v_{ei}^2}\right)^{1/2} \qquad (6)$$

where u_{ei} and v_{ei} are the exact values at a i-th node and the summation is carried out over the nodes of the computational domain.

As seen in Fig. 12, the influence of the supports type is not very significant in the present case, the best choice being ellipses. As may be expected, enlarging stencils (that is, increasing the area of supports) improves the accuracy and the rate of the solution errors decrease with h_x. However, it does not necessary mean that, generally, the improving will continue when including more and more nodes in stencils but keeping constant h_x. The situation is similar to that in the finite difference case when truncation errors do not necessary tend to zero for constant mesh size when increasing a number of grid points in a stencil.

Once numerical solutions for displacements are obtained, the corresponding stresses calculations may be viewed as a postprocessing procedure. A rich variety of RBF approximations to derivatives using different stencils

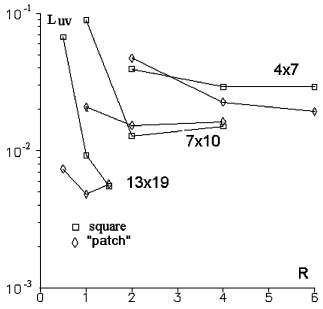

Fig. 14. The problem of a plate with a hole: relative errors of displacements vs. characteristic supports scale R for two supports and three meshes

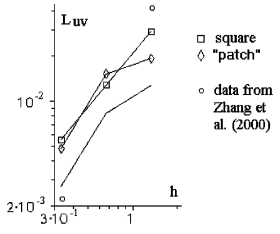

Fig. 15. The problem of a plate with a hole: "saturated" accuracy vs. h for two types of stencils. Solid line without markers corresponds to condensing of nodes near boundaries in the radial direction for elliptical supports

can be used. In the present particular case, finite difference formulas were found to work well.

Figure 13 presents the relative errors in the stresses σ_{xx} and σ_{xy} defined to [32] for the calculations with the elliptical supports.

The next example is an infinite plate with a hole subjected to an uniform traction σ_0 in the x-direction at infinity, the exact solution of the problem can be found, for example in [32]. In the polar coordinates (r, ϕ) it reads

$$u = \frac{\sigma_0}{E}\left[\left(r + \frac{2}{r}\right)\cos\phi + \frac{\nu+1}{2r}\left(1 - \frac{1}{r^2}\right)\cos 3\phi\right]$$

$$v = \frac{\sigma_0}{E}\left[\left(-\nu r + \frac{\nu-1}{r}\right)\sin\phi + \frac{\nu+1}{2r}\left(1 - \frac{1}{r^2}\right)\sin 3\phi\right]$$

Due to symmetry, the domain $0 \le x \le 5,\ \ 0 \le x \le 5$ with the quoter of the hole $x^2 + y^2 < r^2$, $r = 1$ was considered (Fig. 11b). Again, the boundary conditions were extracted from the exact solution. Uniform nodes distributions were used, M and N nodes being placed in the radial and azimuthal directions.

Several types of stencils were assigned to the nodes, to obtain below presented results, the supports which are shown in Fig. 11b are used. They are squares with the characteristic length R as well as the "patches" which are defined by

$$r_0 - R < r < r_0 + R, \quad \phi_0 - \Delta\phi < \phi < \phi_0 + \Delta\phi$$

where $\Delta\phi = 20^\circ$.

Figure 14 shows the E_{uv} displacements errors for three uniform nodes distributions (4×7, 7×10, 13×19) as functions of R. As seen in the Figure, the solution errors decrease with increasing R for a fixed $M \times N$ mesh if $R < R_*(M, N)$ where $R_*(M, N)$ is a "saturation" value. Further increase of R for fixed M and N does not reduce noticeably the errors. It agrees well with the discussion concerning Fig. 12 and is most likely to be due to approaching the limit similar to that deduced from the RBF cardinal interpolation theory dealing with the infinite number of uniformly spaced nodes of rectangular meshes. The behaviour of the "minimal" errors $E_m = E_{uv}(R_*)$ when refining the meshes (that is, when increasing the density of nodes) is shown in Fig. 15 together with the collocation results for the same problem from [32] based on locally supported RBF (CSRBF) with the support size $R = 3$. Condensing the nodes near boundaries in the radial direction yields a large dividend in accuracy of the present calculations as illustrated by the solid curve without markers in Fig. 15.

Figure 16 presents the stress σ_{xx} distribution along y-axis obtained with the stencils "patch" defined on three uniform meshes. In the Figure, noticeable deviation from the exact solution can be seen for very coarse mesh 6×7. However, the accuracy is considerably improved when using more refined 15×19 mesh.

Calculations for the plate with a hole were also carried out using the traction boundary conditions instead of the Dirichlet ones at some boundaries. They were discretized by boundary RBF operators for "one-sided" stencils. As expected, the resulting accuracy was found to be poorer than in the Dirichlet boundary conditions case. Nevertheless, it turns out that it is better than that of the Hermite based collocation method ([32] case 2) for exactly the same problem formulation. The comparison is presented in Fig. 17 where the curves without markers are extracted from [32] (the solid and dashed curves correspond to the CSRBF and globally supported thin plate spline basis functions).

4
Non-linear shell deformations

4.1
Governing equations and problem formulation

As another example of the present RBF technique application, we consider a non-linear shell problem described by the Karman-Fopple equations [10].

Based on the Kirchgoff assumptions, the equations for a plate having thickness h read

$$\frac{\partial^2 u_1}{\partial x^2} + \frac{\partial w}{\partial x}\frac{\partial^2 w}{\partial x^2} + \frac{1+\nu}{2}\left(\frac{\partial^2 u_2}{\partial x \partial y} + \frac{\partial w}{\partial y}\frac{\partial^2 w}{\partial x \partial y}\right) + \frac{1-\nu}{2}\left(\frac{\partial^2 u_1}{\partial y^2} + \frac{\partial w}{\partial x}\frac{\partial^2 w}{\partial y^2}\right) = 0$$

$$\frac{\partial^2 u_2}{\partial y^2} + \frac{\partial w}{\partial y}\frac{\partial^2 w}{\partial y^2} + \frac{1+\nu}{2}\left(\frac{\partial^2 u_1}{\partial x \partial y} + \frac{\partial w}{\partial x}\frac{\partial^2 w}{\partial x \partial y}\right) + \frac{1-\nu}{2}\left(\frac{\partial^2 u_2}{\partial x^2} + \frac{\partial w}{\partial y}\frac{\partial^2 w}{\partial x^2}\right) = 0$$

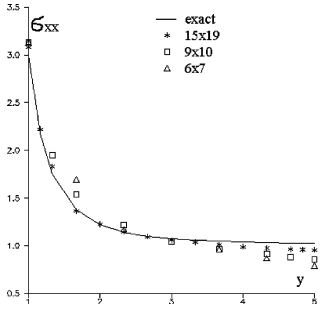

Fig. 16. The problem of a plate with a hole: stress distributions along y axis for different meshes

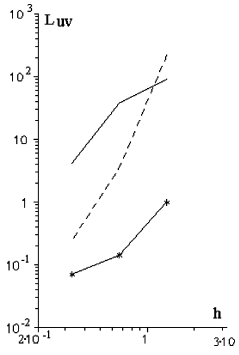

Fig. 17. The problem of a plate with a hole: relative errors of displacement vs. mesh size in the case of traction boundary conditions. The line with markers correspond to the present calculations (saturated values for stencil A). Solid and dashed lines without markers correspond the collocation results of Zhang et al. (2000) obtained with locally and globally supported RBF

$$
\begin{aligned}
D\triangle\triangle w = q + \frac{Eh}{1-\nu^2} \\
\times \left[\left(\frac{\partial u_1}{\partial x} + \nu \frac{\partial u_2}{\partial y} + \frac{1}{2}\left(\frac{\partial w}{\partial x}\right)^2 + \frac{\nu}{2}\left(\frac{\partial w}{\partial y}\right)^2 \right) \frac{\partial^2 w}{\partial x^2} \right. \\
+ \left(\frac{\partial u_2}{\partial y} + \nu \frac{\partial u_1}{\partial x} + \frac{1}{2}\left(\frac{\partial w}{\partial y}\right)^2 + \frac{\nu}{2}\left(\frac{\partial w}{\partial x}\right)^2 \right) \frac{\partial^2 w}{\partial y^2} \\
\left. + (1-\nu)\left(\frac{\partial u_1}{\partial y} + \frac{\partial u_2}{\partial x} + \frac{\partial w}{\partial x}\frac{\partial w}{\partial y} \right) \frac{\partial^2 w}{\partial x \partial y} \right]
\end{aligned}
$$

In the above equations, u_1, u_2, w are the displacements of a plate middle surface corresponding to the Cartesian coordinates x, y, z respectively. It is supposed that the coordinates origin is at the surface, the axis z being normal to it. The constants ν and E are the Poisson coefficient and the Young modulus while $D = Eh^3/(12(1-\nu^2))$ is the cylindrical stiffness.

Consider now the boundary conditions for the system. At a boundary point, four conditions are needed, that is one condition for each of the first two equations and two conditions for the third equation. In the following, simply supported edges or clamped edges will be assumed. In both cases, the boundary conditions for the first two equations and the condition for the third equation look as

$$u_1|_\Gamma = u_2|_\Gamma = w|_\Gamma = 0$$

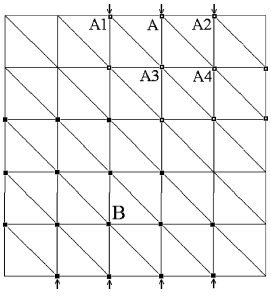

Fig. 18. The stencils for boundary and near-boundary nodes A and B respectively used for derivatives discretizations

The second condition for the third equation in the clamped edges case has the form $\partial w/\partial n = 0$ where $\partial/\partial n = 0$ is the operator of the derivative in the normal to the boundary direction. In the case of simply supported edges, it reads

$$\triangle w + (1-\nu)k\partial w/\partial n = 0$$

where k is the curvature of the boundary. By using the condition, one can avoid, as indicated in [18], a manifestation of the Babuska–Saponjan paradox concerning the difference between the solutions corresponding to round plates and plates with polygon boundaries with the number of vertices tending to infinity.

4.2
RBF-approximation and solution procedure

In the following, an unstructured triangulated grid with a total number of nodes N and a number of boundary nodes N_b will be assumed. Such a grid allows one to deal with complicated geometries.

To approximate the displacements of the middle surface, grid functions $u_{1j}, u_{2j}, w_j, j = 1, \ldots, N$ are introduced. Moreover, we introduce also a grid function $W_j, \quad j = 1, \ldots, N + N_b$ which values are partly coincide with w_j ($W_j = w_j, \ j = 1, \ldots, N$). Its another part (for $j = N+1, \ldots, N+N_b$) is supposed to be approximations to normal derivatives $(\partial w/\partial n)|_\Gamma$ at boundary nodes.

The first two equations contain first and second derivatives. To approximate them, the differencing formulas presented in Sect. 2 and applied to the "simple" and "enlarged" stencils defined in Subsection 3.1 for triangulated meshes were used.

Figure 18 shows an example of a stencil for a boundary node A, the nodes for which normal derivatives are used being indicated by arrows. The total number of the nodes included in the stencil is equal to 10. The sixteen nodes stencil with center B used for the fourth derivatives discretization is also shown in Fig. 18.

Using boundary operators, the governing equations can be discretized at each internal node resulting in algebraic systems for the vector-valued nodal functions u_1, u_2 and W which can be cast in the form

$$
\begin{aligned}
L_{11}u_1^{n+1} + L_{12}u_2^{n+1} &= f_1(W^n) \\
L_{21}u_1^{n+1} + L_{22}u_2^{n+1} &= f_2(W^n) \\
LW^{n+1} &= f(u_1^{n+1}, u_2^{n+1}, W^n)
\end{aligned}
$$

Table 1. Simply supported edges, "simple" stencils

Q	$N = 6$	$N = 11$	$N = 21$
L	0.639573	0.678979	0.690896
0.5	0.280534	0.292354	0.295916
1	0.462217	0.474779	0.478693
1.5	0.589018	0.60072	0.604539
2	0.686973	0.697728	0.701409
3	0.836304	0.84545	0.848888
4	0.950796	0.958674	0.961922
5	1.04496	1.0518	1.05489
6	1.12568	1.13163	1.13459

Table 2. Simply supported edges, "enlarged" stencils

Q	$N = 6$	$N = 11$	$N = 21$
L	0.701446	0.695955	0.695317
0.5	0.299712	0.297611	0.297283
1	0.484001	0.480913	0.480302
1.5	0.6107	0.60702	0.606209
2	0.708165	0.704068	0.703107
3	0.85646	0.851792	0.850619
4	0.970048	0.964994	0.963676
5	1.06342	1.05809	1.05667
6	1.14343	1.13788	1.13638

where L_{11}, L_{12}, L_{21}, L_{22}, L are the operators approximating linear parts of the equations while the right hand sides contain non-linear operators, n being the iteration count. Thus, the solution procedure consists of solving the linear systems for u_1 and u_2 during $(n+1)$th iteration with known W^n values, calculating f in the third equation and, finally, solving the linear system for W^{n+1}.

Considering the above systems in more detail, the first two vector equations form a linear system with $2N$ scalar equations of which $2N_b$ equations correspond to the boundary nodes. The third vector equation is the linear system for W^{n+1} containing $N + N_b$ scalar equations of which N_b, N_b and $N - N_b$ equations correspond to the boundary values of w, the approximations to $\partial w/\partial n|_\Gamma$ and internal nodes respectively.

4.3
Examples of calculations

As a test problem, consider bending of a round plate with simply supported or clamped edges under uniform loading. Due to the central symmetry, the highly accurate solution can be obtained by solving ordinary differential equations. The solution will be used as a reference one. Though the present technique is a meshless one, it is natural to use, as in the previous cases, nodes resulting from a triangulation shown in Fig. 5. The number of nodes N along the radial directions were chosen to be $N = 6, 11, 21$, the corresponding h^*-values being $h^* = 0.2, 0.1, 0.05$.

In Tables 1–4, the center displacements of the plate $W = w_{\text{center}}/h$ are presented for various values of the dimensionless load $Q = q(R/h)^4/E$ and the above mentioned values of N, h and R being the plate thickness and

Table 3. Clamped edges, "simple" stencils

Q	$N = 6$	$N = 11$	$N = 21$
1	0.157253	0.164588	0.16704
2	0.304789	0.316933	0.320936
4	0.554994	0.568998	0.57538
6	0.751259	0.762516	0.766192
8	0.909514	0.917129	0.919709

Table 4. Clamped edge, "enlarged" stencils

Q	$N = 6$	$N = 11$	$N = 21$	Ref
1	0.165359	0.167443	0.167888	0.167849
2	0.319058	0.321727	0.322344	0.322495
4	0.575368	0.575014	0.575242	0.576245
6	0.773659	0.768236	0.767733	0.769561
8	0.932794	0.922223	0.920965	0.923383

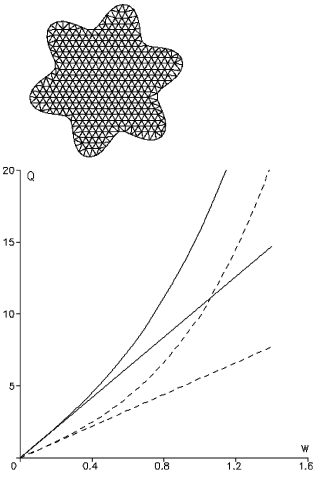

Fig. 19. A mesh for a plate with complicated geometry and Q vs W curves. Solid and dashed lines correspond to simply supported and clamped edge

the plate radius respectively. The Poisson coefficient is assumed to be 0.3. For comparison, the reference solution (column "ref") and the results for the linear case with $Q = 1$ (string "L" in Tables 1, 2) are also included in the Tables. It should be noted that the exact solution for the latter case is $W = 0.695625$.

As can be seen, the difference between the RBF and reference solution does not exceed 0.5% for $N = 21$ in the case of the "simple" stencil and 0.2% for $N = 11$ in the case of the "enlarged" stencil.

As an example of more complicated geometry, Fig. 19 presents the dependence "W vs. Q where W and Q are the above defined variables. The plate boundary is given by $r = R(1 + \cos(6\phi)/5)$ in the polar coordinates (r, ϕ), the nodes distribution being shown in the figure. One can see considerable difference of the results obtained in the frameworks of linear and non-linear theory.

5
Conclusions

A way of using radial basis functions for solving PDEs has been described. Its essence is constructing approximations to derivatives at each node based on RBF interpolants for a limited number of neighbour nodes forming a stencil in the finite difference sense. In contrast to the collocation approach, PDEs are approximated rather than satisfied at nodes in computational domains.

The approach has the potential for minimizing the drawback related to ill-conditioned systems for RBF coefficients and providing reasonable solutions accuracy for relatively modest numbers of nodes. It allows one to be quite flexible by choosing stencils for distinct nodes and different types of derivatives.

The technique has been applied to several elasticity problems. The numerical experiments confirmed the above theoretical expectations. Comparisons with the exact solutions showed that quite accurate numerical solutions can be obtained using relatively low-density nodes distributions. At the same time, further investigations into operating properties of the RBF "finite difference mode" are needed. In particular, optimal strategies of defining stencils can be viewed as the subject of the study.

References

1. **Babuska I, Scapolla T** (1989) Benchmark computation and performance evaluation for a rhombic plate bending problem. Int. J. Numer. Meth. Eng. 28: 155–179
2. **Beatson RK, Cherrie JB, Monal CT** (1999) Fast fitting of radial basis functions. Methods based on preconditioned GMRES iteration. Adv. Comput. Math. 11: 253–270
3. **Belotserkovskii OM, Kholodov AS** (1999) Majorizing schemes on unstructured grids in the space indeterminate coefficients. Comput. Math. Math. Phys. 39: 1730–1747
4. **Belytchko T, Krongaus Y, Organ D, Fleming M, Krysl P** (1996) Meshless methods: An overview and recent developments. Comput. Meth. Appl. Eng. 139: 3–47
5. **Buhmann MD** (1990) Multivariate cardinal interpolation with radial-basis functions. Constructive Approximations 6: 225–255
6. **Buhmann MD** (1998) Radial functions on compact support. Proc. Edinburg Math. Soc. 41: 33–46
7. **Fasshauer G** (1996) Solving partial differential equations with collocation with radial basis functions. In: LeMehaute A, Robut C, Shumaker LL (eds), Chamonix proceedings Vanderbilt University Press, Nashville, TN, 1–8
8. **Franke C, Schaback R** (1998) Solving partial differential equations by collocation using radial basis functions. Appl. Math. Comput. 93: 73–82
9. **George A, Liu JW-H** (1981) Computer Solution of Large Sparse Positive Definite Systems. New Jercey: Prentice-Hall
10. **Grigoluk EI, Mamai VI** (1997) Unlinear deformation of thin-wall constructions. Moscow: Nauka Fizmatlit
11. **Hardy RL** (1990) Theory and applications of multiquadric-biharmonic method. Comput. Math. Appl. 19: 163–208
12. **Kansa EJ** (1990) Multiquadrics – a scattered data approximation scheme with applications to fluid dynamics – II: Solutions to parabolic, hyperbolic and elliptic partial differential equation. Comput. Math. Appl. 19: 147–161
13. **Kansa EJ, Carlson RE** (1995) Radial basis function: a class of grid-free scattered data approximations. Comput. Fluid Dynamics. J. 3: 479–496
14. **Kansa EJ, Hon YC** (2000) Circumventing the ill-conditioning problem with multiquadric radial basis functions: Applications to elliptic partial differential equations. Comput. Math. Appl. 39: 123–137
15. **Lizka T, Orkitz J** (1980) The finite difference method at arbitrary irregular grids and its application in applied mechanics. Comput. Struct. 11: 83–95
16. **Madych WR, Nelson SA** (1989) Error bounds for multiquadric interpolation. In: Chui CK, Shumaker LL, Wards JW (eds), Approximation theory VI Academic Press, NY
17. **Marchuk GI, Agoshkov VI** (1981) Introduction to projective-difference methods. Moscow: Nauka
18. **Mazja VG, Nazarov SA** (1986) Paradoxes of the solutions of boundary value problem on the smooth domain approximated by polygons. Izv. Akad. Nauk USSR, Ser. Mat. 50: 1156–1177
19. **Morley LSD** (1963) Skew plates and Structures. International Series of Monographs in Aeronautics. New York: McMillan
20. **Perrone N, Kao R** (1975) A general finite difference method for arbitrary meshes. Comput. Struct. 5: 45–58
21. **Sharan M, Kansa EJ, Gupta S** (1997) Applications of the multiquadric method for the solution of elliptic partial differential equations. Appl. Math. Comput. 84: 275–302
22. **Timoshenko SP, Goodier SN** (1970) Theory of elasticity, 3rd edn. McGraw-Hill, New York
23. **Tolstykh AI** (1994) High accuracy non-centered compact difference schemes for fluid dynamics applications. Singapore, World Scientific
24. **Tolstykh AI** (2000) On using RBF-based differencing formulas for unstructured and mixed structured-unstructured grid calculations. In: Proceedings of 16th IMACS World Congress, Lausanne
25. **Vlasov VI, Volkov DB** (1995) Multypole method for solving Poisson equation in domains with rounded angles. Zh. Vychisl. Mat. Mat. Fiz. 35: 867–872
26. **Wendland H** (1995) Piecewise polynomial, positive definite and compactly supported radial basis functions of minimal degree. Adv. Comput. Math. 4: 386–396
27. **Wong SM, Hon YC, Li TS, Chug SL, Kansa EJ** (1999) Multizone decomposition of time dependent problems using the multiquadric scheme. Comput. Math. Appl. 37: 23–45
28. **Wu Z, Shaback R** (1993) Local error estimates for radial basis function interpolation of scattered data. IMA J. Numer. Anal. 13: 13–27
29. **Wu Z** (1995) Compactly supported positive definite radial functions. Adv. Comput. Math. 4: 283–292
30. **Wu Z** (1998) Solving PDE with radial basis function and the error estimation. In: Chen Z, Li Y, Micchelli CA, Xu Y, Dekker M, Guang Zhou (eds) Advances in Computational Mathematic Lecture Notes on Pure and Applied Mathematics 202
31. **Zerroukat MA** (1998) Fast boundary element algorithm for time-dependant potential problems. Appl. Math. Modelling 22: 183–196
32. **Zhang X, Song KZ, Lu MW, Liu X** (2000) Meshless methods based on collocation with radial basis functions. Comput. Mech. 26: 333–343